


Cite this: *RSC Adv.*, 2017, 7, 25325

# Synthesis and adsorption properties of $[\text{Cu}(\text{L})_2(\text{H}_2\text{O})]\text{H}_2[\text{Cu}(\text{L})_2(\text{P}_2\text{Mo}_5\text{O}_{23})] \cdot 4\text{H}_2\text{O}/\text{Fe}_3\text{O}_4$ nanocomposites†

Ning Fang, Yu-Mei Ji, Chun-Yan Li, Yuan-Yuan Wu, Chen-Guang Ma, Hong-Ling Liu \* and Ming-Xue Li\*

Multifunctional  $[\text{Cu}(\text{L})_2(\text{H}_2\text{O})]\text{H}_2[\text{Cu}(\text{L})_2(\text{P}_2\text{Mo}_5\text{O}_{23})] \cdot 4\text{H}_2\text{O}/\text{Fe}_3\text{O}_4$  (HL = pyridine-2-carboxamide) nanocomposites were successfully synthesized by combining  $[\text{Cu}(\text{L})_2(\text{H}_2\text{O})]\text{H}_2[\text{Cu}(\text{L})_2(\text{P}_2\text{Mo}_5\text{O}_{23})] \cdot 4\text{H}_2\text{O}$  and  $\text{Fe}_3\text{O}_4$  nanoparticles. The characterization was performed by Fourier transform infrared spectroscopy (FTIR), transmission electron microscopy (TEM), vibrating sample magnetometry (VSM), X-ray powder diffraction (XRD) and ultraviolet-visible light absorbance spectrometry (UV-vis). The XRD and TEM analyses reveal that the nanocomposites possess high crystallinity with an average particle size of  $\sim 19.43$  nm. The VSM and UV-vis demonstrate excellent superparamagnetic behavior and two well-behaved absorption bands of the nanocomposites. The adsorption activity of the nanocomposites was investigated using methylene blue, gentian violet, safranin T, fuchsin basic, methyl orange and Sudan red (III) as probe molecules, and the results reveal that the  $[\text{Cu}(\text{L})_2(\text{H}_2\text{O})]\text{H}_2[\text{Cu}(\text{L})_2(\text{P}_2\text{Mo}_5\text{O}_{23})] \cdot 4\text{H}_2\text{O}/\text{Fe}_3\text{O}_4$  nanocomposites have selective adsorption behavior for organic dyes. The recycling performance was observed using basic fuchsin, and the results demonstrate that the nanocomposites exhibit good recyclability and high stability. The  $[\text{Cu}(\text{L})_2(\text{H}_2\text{O})]\text{H}_2[\text{Cu}(\text{L})_2(\text{P}_2\text{Mo}_5\text{O}_{23})] \cdot 4\text{H}_2\text{O}/\text{Fe}_3\text{O}_4$  nanocomposites have a promising future for magnetic, optical and biomedical applications.

Received 21st February 2017  
Accepted 12th April 2017

DOI: 10.1039/c7ra02133j

rsc.li/rsc-advances

## 1 Introduction

In recent years, polyoxometalate/nanoparticle nanocomposites (POMs/NPs) based on polyoxometalates and nanoparticles have attracted considerable interest due to their unique properties resulting from the combination of the polyoxometalates and the nanoparticles. Research has been dedicated to the fabrication of POMs/NPs with a wide variety of POMs and NPs such as  $\alpha\text{-K}_6\text{P}_2\text{W}_{18}\text{O}_{62}/\text{Pt}$ ,  $\text{Na}_{12}\text{P}_2\text{W}_{15}\text{O}_{56} \cdot 18\text{H}_2\text{O}/\text{Pt}$ ,  $\text{Na}_9\text{EuW}_{10}\text{O}_{36} \cdot 32\text{H}_2\text{O}/\text{Pt}$ ,  $(\text{NH}_4)_{14}\text{NaP}_5\text{W}_{30}\text{O}_{110} \cdot 31\text{H}_2\text{O}/\text{Fe}_3\text{O}_4$ ,  $\text{H}_3\text{PW}_{12}\text{O}_{40}/\text{TiO}_2$ ,  $\text{H}_6\text{P}_2\text{Mo}_{18}\text{O}_{62}/\text{TiO}_2$ ,  $[\text{SiW}_9\text{V}_3\text{O}_{40}]^{7-}/\text{Bi}_2\text{O}_3$ , and  $\alpha\text{-SiW}_{12}\text{O}_{40}^{4-}/\text{Ag}$  to explore the synergistic properties arising from the nanocomposites.<sup>1–5</sup> POMs/NPs have successfully been employed for biocatalysis,<sup>6</sup> electrocatalysis,<sup>7</sup> photocatalysis,<sup>8</sup> oxidation of alkenes,<sup>9</sup> bio-sensing,<sup>10</sup> and medicinal chemistry.<sup>11</sup> The assembly of POMs/NPs can provide a path for exhibiting their unique properties in many fields, and the complex structure makes them attractive for future study.

Polyoxometalates (POMs) are a well-known class of inorganic clusters consisting of a metal–oxygen framework, which have shown unique physicochemical properties and various applications owing to their highly electronegative and oxo-enriched surfaces, controllable shape and size, tunable acid–base, redox, magnetic, catalytic, and photochemical properties.<sup>12–17</sup> On the other hand, magnetic  $\text{Fe}_3\text{O}_4$  nanoparticles are most widely known for their exceptional physicochemical properties, low cost, non-toxic nature as well as environmentally benign for industrial scale synthesis of fine chemicals.<sup>18</sup> The interdisciplinary integration of POMs and  $\text{Fe}_3\text{O}_4$  nanoparticles has accelerated with fundamental curiosity and promising applications. Previously we have prepared  $\text{Fe}_3\text{O}_4$  nanoparticles and their hybrids for the promising applications of heterogeneous catalysis, biological medicine, magnetofection, photo-therapy after magnetic separation, simultaneous photo-therapy and hyperthermia.<sup>19–22</sup> Herein, we report a facile route for the synthesis of  $[\text{Cu}(\text{L})_2(\text{H}_2\text{O})]\text{H}_2[\text{Cu}(\text{L})_2(\text{P}_2\text{Mo}_5\text{O}_{23})] \cdot 4\text{H}_2\text{O}/\text{Fe}_3\text{O}_4$  nanocomposites using the ultrasonic technique.

Now, a large number of dye-waste water discharged pose a significant threat to the water environment and human health due to their toxicity and even carcinogenicity.<sup>23</sup> It is urgently needed to find desirable adsorption materials, which not only reduce the pollutant organic dyes with high efficiency and low lost, but also realize selective separation and recovery. The use of nanomaterials as efficient catalysts in aqueous medium has

Henan Key Laboratory of Polyoxometalates, Institute of Molecular and Crystal Engineering, College of Chemistry and Chemical Engineering, Henan University, Kaifeng 475004, PR China. E-mail: hlliu@henu.edu.cn; limingxue@henu.edu.cn; Fax: +86-371-23881589

† CCDC 1546213. For crystallographic data in CIF or other electronic format see DOI: 10.1039/c7ra02133j



attracted considerable interests.<sup>24,25</sup> We investigated the adsorption of  $[\text{Cu}(\text{L})_2(\text{H}_2\text{O})]\text{H}_2[\text{Cu}(\text{L})_2(\text{P}_2\text{Mo}_5\text{O}_{23})] \cdot 4\text{H}_2\text{O}/\text{Fe}_3\text{O}_4$  nanocomposites using organic dyes such as methylene blue, gentian violet, safranin T, fuchsin basic, methyl orange and Sudan red (III) as probe molecules. The result reveals that the prepared  $[\text{Cu}(\text{L})_2(\text{H}_2\text{O})]\text{H}_2[\text{Cu}(\text{L})_2(\text{P}_2\text{Mo}_5\text{O}_{23})] \cdot 4\text{H}_2\text{O}/\text{Fe}_3\text{O}_4$  nanocomposites have selective adsorption behavior for organic dyes. The reusability of  $[\text{Cu}(\text{L})_2(\text{H}_2\text{O})]\text{H}_2[\text{Cu}(\text{L})_2(\text{P}_2\text{Mo}_5\text{O}_{23})] \cdot 4\text{H}_2\text{O}/\text{Fe}_3\text{O}_4$  nanocomposites as adsorbent is studied as well, and the results demonstrate that the  $[\text{Cu}(\text{L})_2(\text{H}_2\text{O})]\text{H}_2[\text{Cu}(\text{L})_2(\text{P}_2\text{Mo}_5\text{O}_{23})] \cdot 4\text{H}_2\text{O}/\text{Fe}_3\text{O}_4$  nanocomposites unveil good recyclability and high stability. Based on the experimental observations, the as-synthesized  $[\text{Cu}(\text{L})_2(\text{H}_2\text{O})]\text{H}_2[\text{Cu}(\text{L})_2(\text{P}_2\text{Mo}_5\text{O}_{23})] \cdot 4\text{H}_2\text{O}/\text{Fe}_3\text{O}_4$  nanocomposites could be treated as a promising adsorbent candidate. The outcomes prove that the new  $[\text{Cu}(\text{L})_2(\text{H}_2\text{O})]\text{H}_2[\text{Cu}(\text{L})_2(\text{P}_2\text{Mo}_5\text{O}_{23})] \cdot 4\text{H}_2\text{O}/\text{Fe}_3\text{O}_4$  nanocomposites could be of interest for fundamental studies and potential applications in magnetic, optical and biomedical filed.

## 2 Materials and methods

### 2.1 Materials

Copper(II) perchlorate hexahydrate ( $\text{Cu}(\text{ClO}_4)_2 \cdot 6\text{H}_2\text{O}$ , 98%), pyridine-2-carboxamide ( $\text{C}_{22}\text{H}_{17}\text{ClN}_2$ , 98%), sodium molybdate dihydrate ( $\text{Na}_2\text{MoO}_4 \cdot 2\text{H}_2\text{O}$ , 99%) and phosphoric acid ( $\text{H}_3\text{PO}_4$ , 85%) were purchased from J&K Scientific Ltd. Iron(II) acetylacetonate ( $\text{Fe}(\text{acac})_2$ , 99.9%), poly(ethylene glycol)-*block*-poly(propylene glycol)-*block*-poly(ethylene glycol) (PEO-PPO-PEO,  $M_n = 5800$ ), octyl ether ( $\text{C}_8\text{H}_{17}\text{OC}_8\text{H}_{17}$ , 99%), 1,2-hexadecanediol ( $\text{C}_{14}\text{H}_{29}\text{CH}(\text{OH})\text{CH}_2(\text{OH})$ , 90%), DMF ( $\text{HCON}(\text{CH}_3)_2$ , 99.5%) and solvents such as hexane and ethanol were purchased from Aldrich. All materials were used as received without further processing. Distilled water was used throughout.

### 2.2 Synthesis of $\text{Fe}_3\text{O}_4$ nanoparticles

The  $\text{Fe}_3\text{O}_4$  nanoparticles were synthesized according to the reported literature method.<sup>19–22</sup> A typical experiment was carried out in a 100 mL flask, 0.2541 g of iron(II) acetylacetonate, 0.7859 g of PEO-PPO-PEO as the surfactant, and 0.6468 g of 1,2-hexadecanediol were dissolved in 10 mL octyl ether under vigorous stirring. Subsequently, the reaction mixture was slowly heated to 125 °C within 1 h, homogenized for 1 h at 125 °C, then rapidly heated to 280 °C within 15 min and refluxed at the temperature for 1 h to complete the reaction. After cooling down to room temperature, the black precipitate products was washed with mixed solvents of ethanol/hexane ( $V_{\text{ethanol/hexane}}$  is 2 : 1) several times, and re-dispersed in hexane for further use.

### 2.3 Synthesis of $[\text{Cu}(\text{L})_2(\text{H}_2\text{O})]\text{H}_2[\text{Cu}(\text{L})_2(\text{P}_2\text{Mo}_5\text{O}_{23})] \cdot 4\text{H}_2\text{O}$

The  $[\text{Cu}(\text{L})_2(\text{H}_2\text{O})]\text{H}_2[\text{Cu}(\text{L})_2(\text{P}_2\text{Mo}_5\text{O}_{23})] \cdot 4\text{H}_2\text{O}$  was synthesized using the method similar as the literature method.<sup>26–28</sup> An aqueous solution containing  $\text{Cu}(\text{ClO}_4)_2 \cdot 6\text{H}_2\text{O}$  (0.093 g, 0.25 mmol) and pyridine-2-carboxamide (0.061 g, 0.5 mmol) was stirred at 50 °C for 0.5 h. After cooling to room temperature the solution was added to a 10 mL aqueous solution of  $\text{Na}_2\text{MoO}_4 \cdot 2\text{H}_2\text{O}$  (0.242 g, 1.0 mmol), the pH value was maintained at 3 by

dropwise adding of concentrated  $\text{H}_3\text{PO}_4$  under continuous stirring. Then the mixture was stirred for 0.5 h and then filtered. By filtering the mixture, the powders were stored for the following synthesis. The filtrate was allowed to evaporate at room temperature. After 3 days blue crystals suitable for X-ray studies were filtered off, washed with distilled water and dried in a desiccator at room temperature to give a yield of 38.4% based on Mo. Anal. calc. for  $\text{C}_{24}\text{H}_{34}\text{Cu}_2\text{Mo}_5\text{N}_8\text{O}_{32}\text{P}_2$  (1615.30): C, 17.85; H, 2.12; N, 6.94; Cu, 7.87; Mo, 29.70. Found: C, 17.85; H, 2.14; N, 6.92; Cu, 7.88; Mo, 29.66. IR (KBr,  $\text{cm}^{-1}$ ): 3430 (w), 3082 (m), 1684 (s), 1633 (w), 1565 (m), 1497 (m), 1440 (m), 1307 (w), 1278 (w), 1169 (w), 1133 (m), 1058 (s), 1035 (m), 1003 (m), 928 (s), 904 (s), 758 (m), 682 (s), 525 (w).

### 2.4 Synthesis of $[\text{Cu}(\text{L})_2(\text{H}_2\text{O})]\text{H}_2[\text{Cu}(\text{L})_2(\text{P}_2\text{Mo}_5\text{O}_{23})] \cdot 4\text{H}_2\text{O}/\text{Fe}_3\text{O}_4$

$[\text{Cu}(\text{L})_2(\text{H}_2\text{O})]\text{H}_2[\text{Cu}(\text{L})_2(\text{P}_2\text{Mo}_5\text{O}_{23})] \cdot 4\text{H}_2\text{O}/\text{Fe}_3\text{O}_4$  nanocomposites were prepared by an ultrasonic procedure. A typical synthesis was carried out in a 50 mL beaker,  $\text{Fe}_3\text{O}_4$  nanoparticles (5 mg),  $[\text{Cu}(\text{L})_2(\text{H}_2\text{O})]\text{H}_2[\text{Cu}(\text{L})_2(\text{P}_2\text{Mo}_5\text{O}_{23})] \cdot 4\text{H}_2\text{O}$  powders (50 mg) were added in a beaker containing water (10 mL) and ethanol (10 mL) in sequence and obtained an uniform and turbid liquid by ultrasound about 10 h. After the completion of the reaction, the resulting products was collected using a magnet putting on one side of the beaker to separate them from the turbid liquid. The magnetic products were  $[\text{Cu}(\text{L})_2(\text{H}_2\text{O})]\text{H}_2[\text{Cu}(\text{L})_2(\text{P}_2\text{Mo}_5\text{O}_{23})] \cdot 4\text{H}_2\text{O}/\text{Fe}_3\text{O}_4$  nanocomposites, which was washed with water several times.

### 2.5 Structural characterization and measurements of the nanocomposites

The structures of the synthesized  $\text{Fe}_3\text{O}_4$  nanoparticles,  $[\text{Cu}(\text{L})_2(\text{H}_2\text{O})]\text{H}_2[\text{Cu}(\text{L})_2(\text{P}_2\text{Mo}_5\text{O}_{23})] \cdot 4\text{H}_2\text{O}$  and  $[\text{Cu}(\text{L})_2(\text{H}_2\text{O})]\text{H}_2[\text{Cu}(\text{L})_2(\text{P}_2\text{Mo}_5\text{O}_{23})] \cdot 4\text{H}_2\text{O}/\text{Fe}_3\text{O}_4$  nanocomposites were analyzed by X-ray powder diffraction (XRD, X'Pert Pro) and transmission electron microscopy (TEM, JEOL2010F). The UV-vis spectra were measured by an ultraviolet-visible light absorbance spectrometry (UV-vis, HitachiU4100). In the Fourier transform infrared spectroscopy (FTIR) studies,  $\text{Fe}_3\text{O}_4$  nanoparticles,  $[\text{Cu}(\text{L})_2(\text{H}_2\text{O})]\text{H}_2[\text{Cu}(\text{L})_2(\text{P}_2\text{Mo}_5\text{O}_{23})] \cdot 4\text{H}_2\text{O}$  and  $[\text{Cu}(\text{L})_2(\text{H}_2\text{O})]\text{H}_2[\text{Cu}(\text{L})_2(\text{P}_2\text{Mo}_5\text{O}_{23})] \cdot 4\text{H}_2\text{O}/\text{Fe}_3\text{O}_4$  nanocomposites were separately crushed with a pestle in an agate mortar. The individually crushed material was mixed with KBr in about 1 : 100 proportion. The mixture was then compressed into a 2 mm semi-transparent disk by applying a force of 10 T for 2 min. The Fourier transform infrared spectra were recorded in the wavelength range of 500–4000  $\text{cm}^{-1}$  using an Avatar 360 FTIR spectrometer (FTIR, Nicolet Company, USA). The magnetic properties were subsequently investigated by a vibrating sample magnetometry (VSM, Lakeshore 7300).

### 2.6 Crystallography

Crystallographic data were collected with a Bruker SMART-CCD APEX II diffractometer with graphite-monochromated Mo K $\alpha$  radiation ( $\lambda = 0.71073 \text{ \AA}$ ). The structures were solved by direct methods and refined by full-matrix least squares on  $F^2$  with



**Table 1** Summary of crystal data and refinement results for  $[\text{Cu}(\text{L})_2(\text{H}_2\text{O})]\text{H}_2[\text{Cu}(\text{L})_2(\text{P}_2\text{Mo}_5\text{O}_{23})] \cdot 4\text{H}_2\text{O}$ 

Crystal data	$[\text{Cu}(\text{L})_2(\text{H}_2\text{O})]\text{H}_2[\text{Cu}(\text{L})_2(\text{P}_2\text{Mo}_5\text{O}_{23})] \cdot 4\text{H}_2\text{O}$
Empirical formula	$\text{C}_{24}\text{H}_{34}\text{Cu}_2\text{Mo}_5\text{N}_8\text{O}_{32}\text{P}_2$
$f_w$	1615.30
Cryst syst	Triclinic
Space group	$P\bar{1}$
$T$ (K)	296(2)
$a$ (Å)	10.187(3)
$b$ (Å)	10.918(3)
$c$ (Å)	20.739(5)
$\alpha$ (deg)	82.052(4)
$\beta$ (deg)	89.700(5)
$\gamma$ (deg)	88.467(5)
$V$ (Å <sup>3</sup> )	2283.6(10)
$Z$	2
$D_c$ (g cm <sup>-3</sup> )	2.335
$\mu$ (mm <sup>-1</sup> )	2.423
Crystal size (mm)	$0.27 \times 0.18 \times 0.15$
$\theta$ (deg)	1.983–25.098
$F(000)$	1556
$hkl$ range	$-12 \leq h \leq 9$ , $-12 \leq k \leq 12$ , $-24 \leq l \leq 24$
GOF on $F^2$	0.999
$R_{\text{int}}$	0.0433
No. param	671
Refl. measured/unique	8012/5810
$R_1, wR_2$ [ $I \geq 2\sigma(I)$ ]	0.0551, 0.1396
$R_1, wR_2$ (all data)	0.0818, 0.1601
$\Delta\rho_{\text{max}}, \Delta\rho_{\text{min}}$ (e Å <sup>-3</sup> )	1.821, -1.678

anisotropic displacement parameters for all non-hydrogen atoms using SHELXTL.<sup>29</sup> The hydrogen atoms are added in idealized geometrical positions. Crystal data, experimental details, and refinement results are listed in Table 1.

## 2.7 Characterization of adsorption activity

The adsorption activities of the nanocomposites were performed in the dark by measuring the adsorption rate of different dye solutions at room temperature. The dye solutions such as methylene blue, gentian violet, safranin T and fuchsin basic, methyl orange and Sudan red (III) were prepared with a concentration of 15 mg L<sup>-1</sup> by dissolving the dye powder in distilled water. The reaction was conducted with 5 mg of  $[\text{Cu}(\text{L})_2(\text{H}_2\text{O})]\text{H}_2[\text{Cu}(\text{L})_2(\text{P}_2\text{Mo}_5\text{O}_{23})] \cdot 4\text{H}_2\text{O}/\text{Fe}_3\text{O}_4$  nanocomposites which is the adsorbents dispersed in 30 mL of 15 mg L<sup>-1</sup> each dye solutions. After stirring, the samples (volume of each is about 5 mL) were drawn out from the reaction beaker every a period of time, centrifuged at 4500 rpm for 10 min and filtered to remove the particles. The filtrate was then analyzed using a UV-vis spectrophotometer (Beijingpuxitongyong TU-1900) to measure the absorption of different dyes.

## 2.8 Characterization of desorption, reusability activities

In order to investigate the regeneration of the adsorbents during the adsorption experiments, a solvent DMF is chosen as the eluents. The stability and reusability of the nanocomposites on removing fuchsin basic were investigated through cycle tests. The fuchsin basic solution was prepared with a concentration of

15 mg L<sup>-1</sup> by dissolving the dye powder in distilled water. The reaction was conducted with 50 mg of the adsorbents dispersed in 20 mL of 15 mg L<sup>-1</sup> fuchsin basic. After each cycle, the adsorbents were separated from aqueous solution by a piece of magnet and washed with a solvent DMF about 20 mL at room temperature to remove the adsorbed fuchsin basic. Then, the regenerated  $[\text{Cu}(\text{L})_2(\text{H}_2\text{O})]\text{H}_2[\text{Cu}(\text{L})_2(\text{P}_2\text{Mo}_5\text{O}_{23})] \cdot 4\text{H}_2\text{O}/\text{Fe}_3\text{O}_4$  nanocomposites were added to the initial dye solution of fuchsin basic (20 mL of 15 mg L<sup>-1</sup>). The concentrations of fuchsin basic solution were determined by measuring the absorbance through a UV-vis spectrophotometer (Beijingpuxitongyong TU-1900).

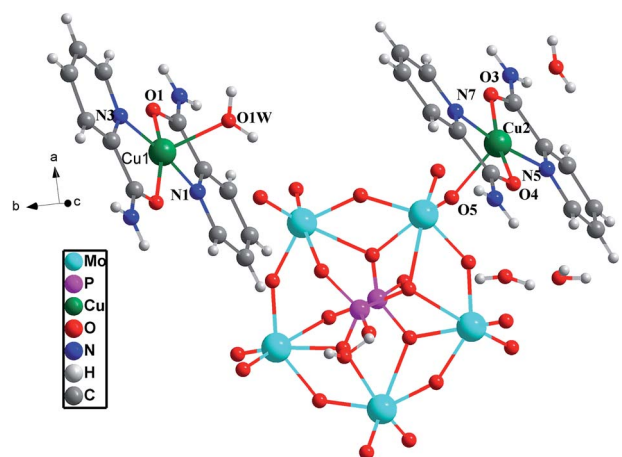
## 3 Results and discussion

### 3.1 Crystal structure description of compound $[\text{Cu}(\text{L})_2(\text{H}_2\text{O})]\text{H}_2[\text{Cu}(\text{L})_2(\text{P}_2\text{Mo}_5\text{O}_{23})] \cdot 4\text{H}_2\text{O}$

Selected bond distances and angles of  $[\text{Cu}(\text{L})_2(\text{H}_2\text{O})]\text{H}_2[\text{Cu}(\text{L})_2(\text{P}_2\text{Mo}_5\text{O}_{23})] \cdot 4\text{H}_2\text{O}$  are given in Table 2. The molecular structures along with the atom numbering scheme are depicted in Fig. 1.

**Table 2** Selected bond lengths (Å) and angles (deg) for  $[\text{Cu}(\text{L})_2(\text{H}_2\text{O})]\text{H}_2[\text{Cu}(\text{L})_2(\text{P}_2\text{Mo}_5\text{O}_{23})] \cdot 4\text{H}_2\text{O}$ 

$[\text{Cu}(\text{L})_2(\text{H}_2\text{O})]\text{H}_2[\text{Cu}(\text{L})_2(\text{P}_2\text{Mo}_5\text{O}_{23})] \cdot 4\text{H}_2\text{O}$			
Cu(1)–O(1)	1.967(6)	Cu(2)–O(3)	1.929(6)
Cu(1)–O(2)	1.959(6)	Cu(2)–O(4)	1.949(6)
Cu(1)–N(1)	1.964(7)	Cu(2)–O(5)	2.236(6)
Cu(1)–N(3)	1.987(8)	Cu(2)–N(5)	1.985(7)
Cu(1)–O(1W)	2.171(6)	Cu(2)–N(7)	1.958(7)
O(1)–Cu(1)–N(3)	97.1(3)	O(3)–Cu(2)–O(4)	168.9(3)
O(1)–Cu(1)–O(1W)	98.6(3)	O(3)–Cu(2)–O(5)	94.5(3)
O(2)–Cu(1)–O(1)	164.5(3)	O(3)–Cu(2)–N(5)	82.4(3)
O(2)–Cu(1)–N(1)	96.0(3)	O(3)–Cu(2)–N(7)	95.4(3)
N(1)–Cu(1)–N(3)	82.6(3)	O(4)–Cu(2)–O(5)	96.5(3)
O(2)–Cu(1)–O(1W)	96.8(3)	O(4)–Cu(2)–N(5)	98.2(3)
N(1)–Cu(1)–O(1)	82.5(3)	O(4)–Cu(2)–N(7)	82.7(3)
N(1)–Cu(1)–N(3)	173.2(3)	N(5)–Cu(2)–O(5)	81.7(3)
N(1)–Cu(1)–O(1W)	92.1(3)	N(7)–Cu(2)–O(5)	105.7(3)
N(3)–Cu(1)–O(1W)	94.6(3)	N(7)–Cu(2)–N(5)	172.4(3)

**Fig. 1** Structure of  $[\text{Cu}(\text{L})_2(\text{H}_2\text{O})]\text{H}_2[\text{Cu}(\text{L})_2(\text{P}_2\text{Mo}_5\text{O}_{23})] \cdot 4\text{H}_2\text{O}$  with atomic numbering scheme.

Single-crystal X-ray structural analysis exhibits that  $[(\text{CuL}_2)(\text{H}_2\text{O})]\text{H}_2[(\text{CuL}_2)(\text{P}_2\text{Mo}_5\text{O}_{23})]\cdot 4\text{H}_2\text{O}$  crystallizes in  $P\bar{1}$  space group. In addition, Fig. 1a shows that compound  $[(\text{CuL}_2)(\text{H}_2\text{O})]\text{H}_2[(\text{CuL}_2)(\text{P}_2\text{Mo}_5\text{O}_{23})]\cdot 4\text{H}_2\text{O}$  consists of  $[(\text{CuL}_2)(\text{P}_2\text{Mo}_5\text{O}_{23})]^{4-}$  polyanion,  $[\text{CuL}_2]^{2+}$  complex fragments and four water molecules in the structural unit of compound  $[(\text{CuL}_2)(\text{H}_2\text{O})]\text{H}_2[(\text{CuL}_2)(\text{P}_2\text{Mo}_5\text{O}_{23})]\cdot 4\text{H}_2\text{O}$ . As is well known, the  $\text{P}_2\text{Mo}_5$  cluster can be viewed as two  $\{\text{PO}_4\}$  tetrahedral capping either side of an irregular ring of five distorted  $\{\text{MoO}_6\}$  octahedral linked by one corner-shared and four edge-shared contacts. Each phosphate subunit shares three oxo-groups with the molybdate ring. One of these oxo-groups adopts a  $\mu_2$ -bridging mode, linking one molybdenum atom and a phosphorus atom; while the other two adopt a  $\mu_3$ -bridging mode, linking two molybdenum atoms and a phosphorus atom.<sup>30</sup> Each of two Cu atoms adopts a five-coordinated distorted  $\{\text{CuN}_2\text{O}_3\}$  square-pyramidal geometry surrounded by two pyridine-2-carboxamide ligands and one O atom from  $\text{P}_2\text{Mo}_5$  cluster or one water, respectively. The Cu(1) is coordinated by two N (amide) atoms with Cu–N bond lengths of 1.968(9)–1.970(9) Å, two O (amide) atoms with Cu–O bond lengths of 1.958(7)–1.960(7) Å and one O (aqua) atom with Cu–Ow bond lengths of 2.169(7) Å. The Cu(2) atom is coordinated by two N (amide) atoms with Cu–N bond lengths of 1.961(9)–1.978(9) Å, one O atom of  $\{\text{MoO}_6\}$  octahedron with Cu–O bond lengths of 2.231(7) Å, and two O (amide) atom with Cu–O bond lengths of 1.930(7)–1.945(7) Å.<sup>31</sup>

### 3.2 IR spectroscopy

Fig. 2 compares the FTIR spectra of  $\text{Fe}_3\text{O}_4$  nanoparticles,  $[(\text{CuL}_2)(\text{H}_2\text{O})]\text{H}_2[(\text{CuL}_2)(\text{P}_2\text{Mo}_5\text{O}_{23})]\cdot 4\text{H}_2\text{O}$  and  $[(\text{CuL}_2)(\text{H}_2\text{O})]\text{H}_2[(\text{CuL}_2)(\text{P}_2\text{Mo}_5\text{O}_{23})]\cdot 4\text{H}_2\text{O}/\text{Fe}_3\text{O}_4$  nanocomposites. In Fig. 2b, the  $\text{Fe}_3\text{O}_4$  nanoparticles show one strong characteristic band at the position of  $600\text{ cm}^{-1}$  which is associated with the stretching vibration mode of Fe–O.<sup>32–34</sup> The IR spectrum of  $[(\text{CuL}_2)(\text{H}_2\text{O})]\text{H}_2[(\text{CuL}_2)(\text{P}_2\text{Mo}_5\text{O}_{23})]\cdot 4\text{H}_2\text{O}$  has been depicted in Fig. 2c. It is evident that the characteristic band at  $3378\text{ cm}^{-1}$  is attributed to the O–H stretching vibration of water, while the peaks at  $3072\text{ cm}^{-1}$  are related to the  $\nu(\text{N–H})$  of pyridine-2-carboxamide. A series of strong bands in the range of  $1684\text{--}1133\text{ cm}^{-1}$  is also associated with pyridine-2-carboxamide. Bands in the region of  $1120\text{--}1008\text{ cm}^{-1}$  are assigned to  $\nu(\text{P–O})$  stretching vibration.<sup>35,36</sup> The peaks at  $908\text{ cm}^{-1}$  and  $672\text{ cm}^{-1}$  are attributed to  $\nu(\text{Mo}=\text{O}_d)$  and  $\nu(\text{Mo–O–Mo})$ , respectively.<sup>36</sup> As given in Fig. 2a, these characteristic vibration and bending modes reappear in the FTIR spectrum of the  $[(\text{CuL}_2)(\text{H}_2\text{O})]\text{H}_2[(\text{CuL}_2)(\text{P}_2\text{Mo}_5\text{O}_{23})]\cdot 4\text{H}_2\text{O}/\text{Fe}_3\text{O}_4$ , but instead shifting to the positions of  $3389\text{ cm}^{-1}$  for the O–H stretching vibration and  $3174\text{ cm}^{-1}$  for the  $\nu(\text{N–H})$  of pyridine-2-carboxamide. The result is that  $\text{Fe}_3\text{O}_4$  and  $[(\text{CuL}_2)(\text{H}_2\text{O})]\text{H}_2[(\text{CuL}_2)(\text{P}_2\text{Mo}_5\text{O}_{23})]\cdot 4\text{H}_2\text{O}$  are existed in  $[(\text{CuL}_2)(\text{H}_2\text{O})]\text{H}_2[(\text{CuL}_2)(\text{P}_2\text{Mo}_5\text{O}_{23})]\cdot 4\text{H}_2\text{O}/\text{Fe}_3\text{O}_4$  nanocomposites, which demonstrates the synthesis of  $[(\text{CuL}_2)(\text{H}_2\text{O})]\text{H}_2[(\text{CuL}_2)(\text{P}_2\text{Mo}_5\text{O}_{23})]\cdot 4\text{H}_2\text{O}/\text{Fe}_3\text{O}_4$  nanocomposites.

### 3.3 UV-vis spectroscopy

The optical property of  $[(\text{CuL}_2)(\text{H}_2\text{O})]\text{H}_2[(\text{CuL}_2)(\text{P}_2\text{Mo}_5\text{O}_{23})]\cdot 4\text{H}_2\text{O}/\text{Fe}_3\text{O}_4$  were assessed by UV-visible absorption spectroscopy. Fig. 3a–c shows the UV-vis spectra of  $[(\text{CuL}_2)(\text{H}_2\text{O})]\text{H}_2[(\text{CuL}_2)(\text{P}_2\text{Mo}_5\text{O}_{23})]\cdot 4\text{H}_2\text{O}/\text{Fe}_3\text{O}_4$  nanocomposites,  $[(\text{CuL}_2)(\text{H}_2\text{O})]\text{H}_2[(\text{CuL}_2)(\text{P}_2\text{Mo}_5\text{O}_{23})]\cdot 4\text{H}_2\text{O}$

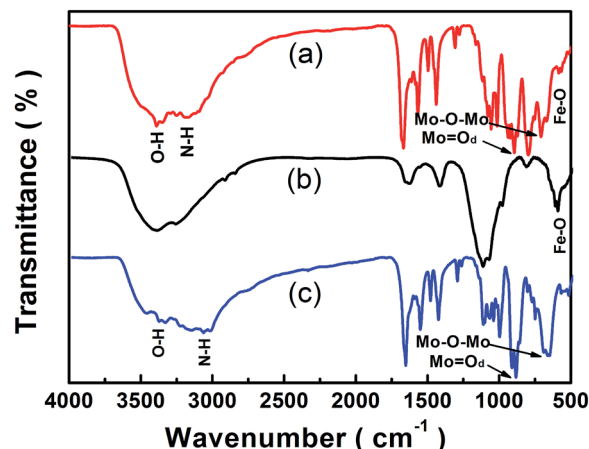


Fig. 2 FTIR spectra of  $[(\text{CuL}_2)(\text{H}_2\text{O})]\text{H}_2[(\text{CuL}_2)(\text{P}_2\text{Mo}_5\text{O}_{23})]\cdot 4\text{H}_2\text{O}/\text{Fe}_3\text{O}_4$  (a),  $\text{Fe}_3\text{O}_4$  (b) and  $[(\text{CuL}_2)(\text{H}_2\text{O})]\text{H}_2[(\text{CuL}_2)(\text{P}_2\text{Mo}_5\text{O}_{23})]\cdot 4\text{H}_2\text{O}$  (c).

$[(\text{CuL}_2)(\text{H}_2\text{O})]\text{H}_2[(\text{CuL}_2)(\text{P}_2\text{Mo}_5\text{O}_{23})]\cdot 4\text{H}_2\text{O}$  and  $\text{Fe}_3\text{O}_4$  dispersed in  $\text{H}_2\text{O}$ . Apparently, in Fig. 3b,  $[(\text{CuL}_2)(\text{H}_2\text{O})]\text{H}_2[(\text{CuL}_2)(\text{P}_2\text{Mo}_5\text{O}_{23})]\cdot 4\text{H}_2\text{O}$  shows two of absorption bands, and the absorption bands observed around 211 nm and 264 nm, which are attributed to the charge-transfer of  $\text{O}_t \rightarrow \text{Mo}$  and  $\text{O}_b \rightarrow \text{Mo}$ , respectively.<sup>37</sup> As given in Fig. 3c, in the ultraviolet and visible light area,  $\text{Fe}_3\text{O}_4$  nanoparticles have no obvious absorption bands. Clearly, in Fig. 3a, there are two kinds of absorption bands, one at about 210 nm and the other at about 265 nm, both from  $[(\text{CuL}_2)(\text{H}_2\text{O})]\text{H}_2[(\text{CuL}_2)(\text{P}_2\text{Mo}_5\text{O}_{23})]\cdot 4\text{H}_2\text{O}$ , the peak pattern of  $[(\text{CuL}_2)(\text{H}_2\text{O})]\text{H}_2[(\text{CuL}_2)(\text{P}_2\text{Mo}_5\text{O}_{23})]\cdot 4\text{H}_2\text{O}/\text{Fe}_3\text{O}_4$  nanocomposites is similar to that of  $[(\text{CuL}_2)(\text{H}_2\text{O})]\text{H}_2[(\text{CuL}_2)(\text{P}_2\text{Mo}_5\text{O}_{23})]\cdot 4\text{H}_2\text{O}$ , and the position of the two peaks is nearly alike, and coming about shift slightly is due to the existence of  $\text{Fe}_3\text{O}_4$  nanoparticles.

### 3.4 TEM morphology and particle size distribution of $[(\text{CuL}_2)(\text{H}_2\text{O})]\text{H}_2[(\text{CuL}_2)(\text{P}_2\text{Mo}_5\text{O}_{23})]\cdot 4\text{H}_2\text{O}/\text{Fe}_3\text{O}_4$

The morphology, nanostructure, particle size and size distribution of the prepared  $[(\text{CuL}_2)(\text{H}_2\text{O})]\text{H}_2[(\text{CuL}_2)(\text{P}_2\text{Mo}_5\text{O}_{23})]\cdot 4\text{H}_2\text{O}/\text{Fe}_3\text{O}_4$

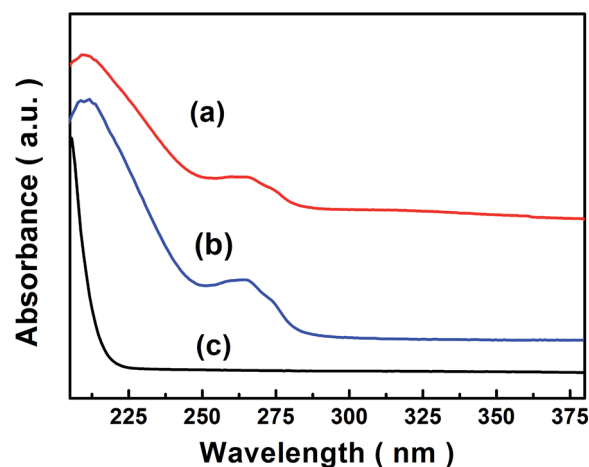


Fig. 3 UV-visible absorbance spectra of  $[(\text{CuL}_2)(\text{H}_2\text{O})]\text{H}_2[(\text{CuL}_2)(\text{P}_2\text{Mo}_5\text{O}_{23})]\cdot 4\text{H}_2\text{O}/\text{Fe}_3\text{O}_4$  (a),  $[(\text{CuL}_2)(\text{H}_2\text{O})]\text{H}_2[(\text{CuL}_2)(\text{P}_2\text{Mo}_5\text{O}_{23})]\cdot 4\text{H}_2\text{O}$  (b) and  $\text{Fe}_3\text{O}_4$  (c) dispersed in  $\text{H}_2\text{O}$ .





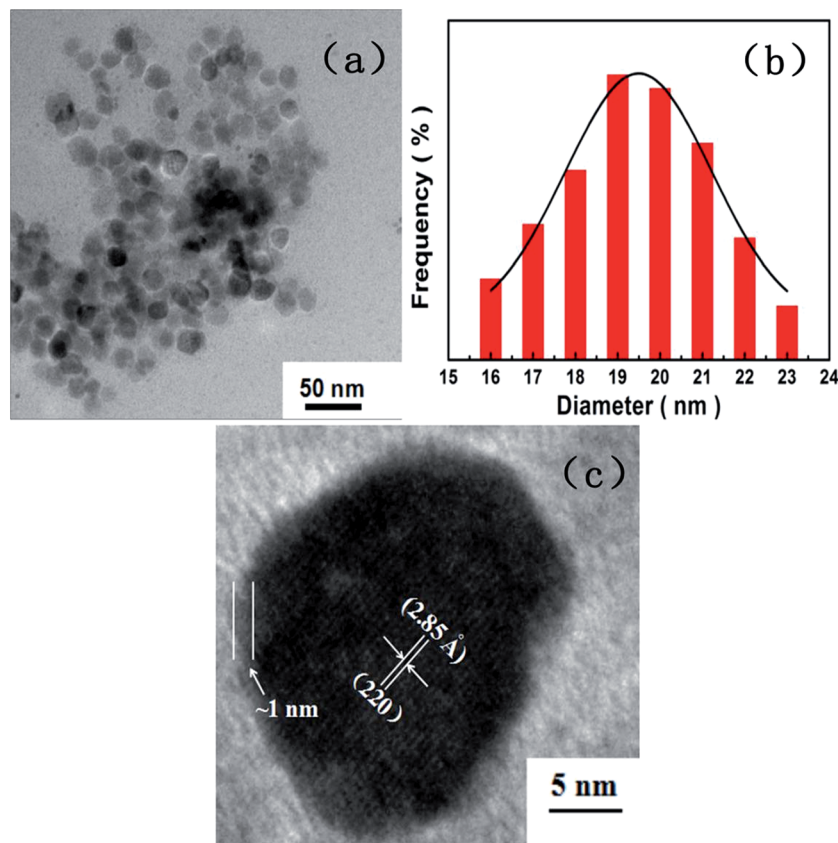


Fig. 4 TEM analyses (a), particle size histogram with Gaussian fit (b) and HRTEM analyses of  $[\text{Cu}(\text{L})_2(\text{H}_2\text{O})]\text{H}_2[\text{Cu}(\text{L})_2(\text{P}_2\text{Mo}_5\text{O}_{23})] \cdot 4\text{H}_2\text{O}/\text{Fe}_3\text{O}_4$  nanocomposites (c).

nanocomposites were recorded by TEM and HRTEM. As given in Fig. 4a, the obtained  $[\text{Cu}(\text{L})_2(\text{H}_2\text{O})]\text{H}_2[\text{Cu}(\text{L})_2(\text{P}_2\text{Mo}_5\text{O}_{23})] \cdot 4\text{H}_2\text{O}/\text{Fe}_3\text{O}_4$  nanocomposites are virtually uniform and nearly spherical in shape with seldom aggregation. The histograms in Fig. 4b shows the size distribution of  $[\text{Cu}(\text{L})_2(\text{H}_2\text{O})]\text{H}_2[\text{Cu}(\text{L})_2(\text{P}_2\text{Mo}_5\text{O}_{23})] \cdot 4\text{H}_2\text{O}/\text{Fe}_3\text{O}_4$  nanocomposites, which are reasonably described by the Gaussian function, showing tight size distribution with average sizes of approximately 19.43 nm in diameter. Fig. 4c represents the HRTEM image of a single  $[\text{Cu}(\text{L})_2(\text{H}_2\text{O})]$

$\text{H}_2[\text{Cu}(\text{L})_2(\text{P}_2\text{Mo}_5\text{O}_{23})] \cdot 4\text{H}_2\text{O}/\text{Fe}_3\text{O}_4$  nanocomposite. As labeled, the spacing of 2.85 Å corresponds to the (220) reflection of the  $\text{Fe}_3\text{O}_4$  phase. Moreover, with a higher magnification than in Fig. 4a of the same sample, a thin layer with ~1 nm uneven thickness is clearly observed in Fig. 4c. We think that this similarly may be the example of observation of such kind of  $[\text{Cu}(\text{L})_2(\text{H}_2\text{O})]\text{H}_2[\text{Cu}(\text{L})_2(\text{P}_2\text{Mo}_5\text{O}_{23})] \cdot 4\text{H}_2\text{O}/\text{Fe}_3\text{O}_4$  core-shell structure.<sup>38,39</sup>

### 3.5 XRD patterns

As shown in Fig. 5, the structure of the  $[\text{Cu}(\text{L})_2(\text{H}_2\text{O})]\text{H}_2[\text{Cu}(\text{L})_2(\text{P}_2\text{Mo}_5\text{O}_{23})] \cdot 4\text{H}_2\text{O}/\text{Fe}_3\text{O}_4$  nanocomposites was recorded by XRD

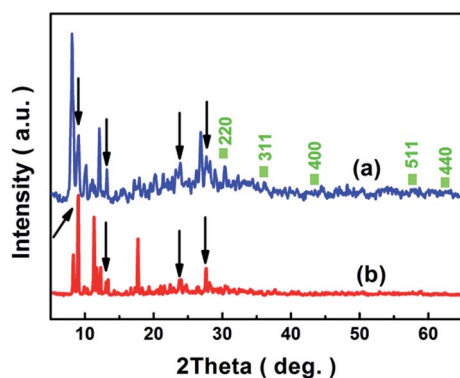


Fig. 5 XRD patterns for  $[\text{Cu}(\text{L})_2(\text{H}_2\text{O})]\text{H}_2[\text{Cu}(\text{L})_2(\text{P}_2\text{Mo}_5\text{O}_{23})] \cdot 4\text{H}_2\text{O}/\text{Fe}_3\text{O}_4$  (a),  $[\text{Cu}(\text{L})_2(\text{H}_2\text{O})]\text{H}_2[\text{Cu}(\text{L})_2(\text{P}_2\text{Mo}_5\text{O}_{23})] \cdot 4\text{H}_2\text{O}$  (b) and squares for the JCPDS of  $\text{Fe}_3\text{O}_4$ .

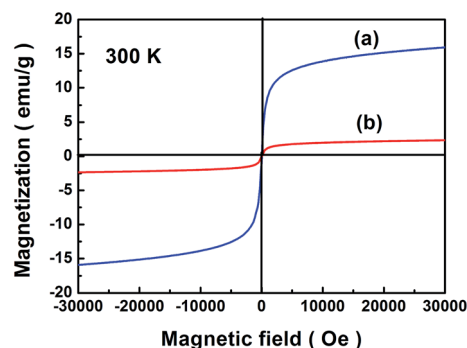


Fig. 6 Magnetic measurements of  $\text{Fe}_3\text{O}_4$  nanoparticles (a) and  $[\text{Cu}(\text{L})_2(\text{H}_2\text{O})]\text{H}_2[\text{Cu}(\text{L})_2(\text{P}_2\text{Mo}_5\text{O}_{23})] \cdot 4\text{H}_2\text{O}/\text{Fe}_3\text{O}_4$  nanocomposites (b).



and analyzed together with the results of  $\text{Fe}_3\text{O}_4$  and  $[\text{Cu}(\text{L})_2(\text{H}_2\text{O})]\text{H}_2[\text{Cu}(\text{L})_2(\text{P}_2\text{Mo}_5\text{O}_{23})]\cdot 4\text{H}_2\text{O}$ . Fig. 5a represents the diffraction pattern obtained from the  $[\text{Cu}(\text{L})_2(\text{H}_2\text{O})]\text{H}_2[\text{Cu}(\text{L})_2(\text{P}_2\text{Mo}_5\text{O}_{23})]\cdot 4\text{H}_2\text{O}/\text{Fe}_3\text{O}_4$  nanocomposites, in match to the standard diffraction peaks of the corresponding  $\text{Fe}_3\text{O}_4$  (JCPDS No.88-0315), the diffraction peaks positioning at  $30.2^\circ$ ,  $35.6^\circ$ ,  $43.2^\circ$ ,  $57.3^\circ$  and  $62.7^\circ$  are indexed to the (220), (311), (400), (511) and (440) planes

of the  $\text{Fe}_3\text{O}_4$  nanoparticles. Fig. 5b represents the diffraction pattern obtained from the  $[\text{Cu}(\text{L})_2(\text{H}_2\text{O})]\text{H}_2[\text{Cu}(\text{L})_2(\text{P}_2\text{Mo}_5\text{O}_{23})]\cdot 4\text{H}_2\text{O}$ , the diffraction peaks positioning at  $8.8^\circ$ ,  $12.9^\circ$ ,  $23.8^\circ$  and  $27.1^\circ$  also appear in Fig. 5a which are indicated by arrows. In conclusion,  $[\text{Cu}(\text{L})_2(\text{H}_2\text{O})]\text{H}_2[\text{Cu}(\text{L})_2(\text{P}_2\text{Mo}_5\text{O}_{23})]\cdot 4\text{H}_2\text{O}$  and  $\text{Fe}_3\text{O}_4$  are included in  $[\text{Cu}(\text{L})_2(\text{H}_2\text{O})]\text{H}_2[\text{Cu}(\text{L})_2(\text{P}_2\text{Mo}_5\text{O}_{23})]\cdot 4\text{H}_2\text{O}/\text{Fe}_3\text{O}_4$  nanocomposites.

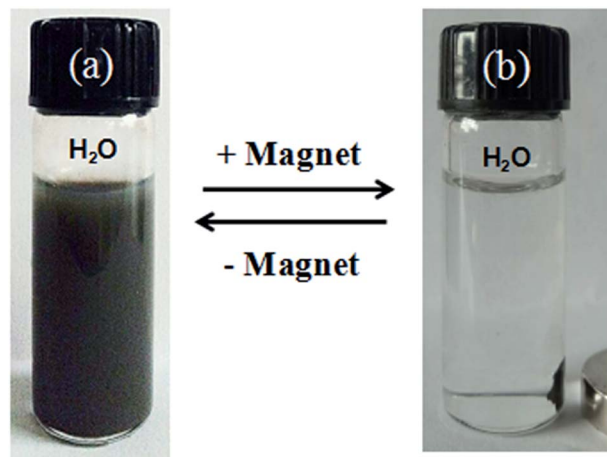


Fig. 7 Photo images of solvent of  $\text{H}_2\text{O}$  dispersion-collection process of the  $[\text{Cu}(\text{L})_2(\text{H}_2\text{O})]\text{H}_2[\text{Cu}(\text{L})_2(\text{P}_2\text{Mo}_5\text{O}_{23})]\cdot 4\text{H}_2\text{O}/\text{Fe}_3\text{O}_4$  nanocomposites.

### 3.6 Magnetic property of $[\text{Cu}(\text{L})_2(\text{H}_2\text{O})]\text{H}_2[\text{Cu}(\text{L})_2(\text{P}_2\text{Mo}_5\text{O}_{23})]\cdot 4\text{H}_2\text{O}/\text{Fe}_3\text{O}_4$

The magnetic property of  $[\text{Cu}(\text{L})_2(\text{H}_2\text{O})]\text{H}_2[\text{Cu}(\text{L})_2(\text{P}_2\text{Mo}_5\text{O}_{23})]\cdot 4\text{H}_2\text{O}/\text{Fe}_3\text{O}_4$  nanocomposites was studied by VSM. Fig. 6a and b show the hysteresis curves of  $\text{Fe}_3\text{O}_4$  nanoparticles and  $[\text{Cu}(\text{L})_2(\text{H}_2\text{O})]\text{H}_2[\text{Cu}(\text{L})_2(\text{P}_2\text{Mo}_5\text{O}_{23})]\cdot 4\text{H}_2\text{O}/\text{Fe}_3\text{O}_4$  nanocomposites at 300 K, respectively. It is clear that  $[\text{Cu}(\text{L})_2(\text{H}_2\text{O})]\text{H}_2[\text{Cu}(\text{L})_2(\text{P}_2\text{Mo}_5\text{O}_{23})]\cdot 4\text{H}_2\text{O}/\text{Fe}_3\text{O}_4$  nanocomposites show superparamagnetic behavior with a coercivity tend to  $\sim 9.0$  Oe and magnetization of  $\sim 2.37$  emu  $\text{g}^{-1}$  comparing with a coercivity tend to  $\sim 0$  Oe and magnetization of  $\sim 16.10$  emu  $\text{g}^{-1}$  of  $\text{Fe}_3\text{O}_4$  nanoparticles.

### 3.7 Separation and aggregation process of $[\text{Cu}(\text{L})_2(\text{H}_2\text{O})]\text{H}_2[\text{Cu}(\text{L})_2(\text{P}_2\text{Mo}_5\text{O}_{23})]\cdot 4\text{H}_2\text{O}/\text{Fe}_3\text{O}_4$

Fig. 7 visually demonstrates the separation and aggregation process of the  $[\text{Cu}(\text{L})_2(\text{H}_2\text{O})]\text{H}_2[\text{Cu}(\text{L})_2(\text{P}_2\text{Mo}_5\text{O}_{23})]\cdot 4\text{H}_2\text{O}/\text{Fe}_3\text{O}_4$  nanocomposites in water.<sup>40</sup> Under the influence of an external magnetic field,  $[\text{Cu}(\text{L})_2(\text{H}_2\text{O})]\text{H}_2[\text{Cu}(\text{L})_2(\text{P}_2\text{Mo}_5\text{O}_{23})]\cdot 4\text{H}_2\text{O}/\text{Fe}_3\text{O}_4$

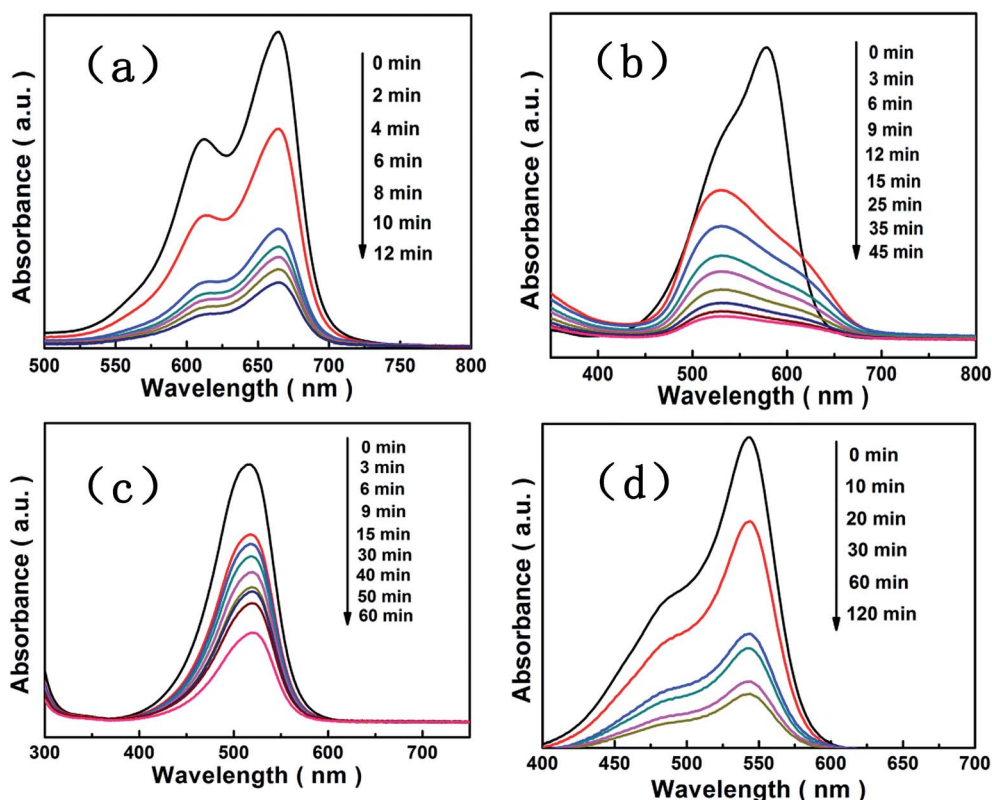


Fig. 8 Adsorption spectra of the methylene blue solution (a), the gentian violet solution (b), the safranin T solution (c) and the fuchsin basic solution (d) under the dark in presence of the  $[\text{Cu}(\text{L})_2(\text{H}_2\text{O})]\text{H}_2[\text{Cu}(\text{L})_2(\text{P}_2\text{Mo}_5\text{O}_{23})]\cdot 4\text{H}_2\text{O}/\text{Fe}_3\text{O}_4$  nanocomposites.



nanocomposites in water change from a purplish grey, homogeneous dispersion (Fig. 7a) to a clear, transparent solution, with the nanocomposites collected by a piece of magnet (Fig. 7b). The collected nanocomposites can be easily and reversibly dispersed by agitation after removal of the magnetic field and the above process can be repeated. The finding that all  $[\text{Cu}(\text{L})_2(\text{H}_2\text{O})]\text{H}_2[\text{Cu}(\text{L})_2(\text{P}_2\text{Mo}_5\text{O}_{23})] \cdot 4\text{H}_2\text{O}/\text{Fe}_3\text{O}_4$  nanocomposites as prepared could be collected by a magnet, leaving no free  $[\text{Cu}(\text{L})_2(\text{H}_2\text{O})]\text{H}_2[\text{Cu}(\text{L})_2(\text{P}_2\text{Mo}_5\text{O}_{23})] \cdot 4\text{H}_2\text{O}$  visible. In other words, we performed magnetic separation and found that all nanocomposites were collected by the magnet because the  $[\text{Cu}(\text{L})_2(\text{H}_2\text{O})]\text{H}_2[\text{Cu}(\text{L})_2(\text{P}_2\text{Mo}_5\text{O}_{23})] \cdot 4\text{H}_2\text{O}/\text{Fe}_3\text{O}_4$  nanocomposites are magnetic and there is no more nanoparticles left-over, so nonmagnetic  $[\text{Cu}(\text{L})_2(\text{H}_2\text{O})]\text{H}_2[\text{Cu}(\text{L})_2(\text{P}_2\text{Mo}_5\text{O}_{23})] \cdot 4\text{H}_2\text{O}$  are not present in the samples.

### 3.8 Adsorption properties

Organic dyes such as methylene blue, gentian violet, safranin T and fuchsin basic are important organic dyes which are widely used as a colorant in textiles and food stuffs the dyes are harmful if swallowed by human beings and animals, causing irritation to the skin, eye and respiratory tract.<sup>41–43</sup> Their breakdown products in the water may be toxic, carcinogenic or mutagenic to life forms, and they have been shown to cause retching, stun, cyanosis, jaundice and tissue necrosis in human. Therefore, an effective and optimal strategy to degrade the dyes rapidly must be developed. In the design of an economical wastewater disposal system, fast adsorption rate is also an important parameter for design and synthesis of the efficient adsorbent.

We investigated the adsorption of  $[\text{Cu}(\text{L})_2(\text{H}_2\text{O})]\text{H}_2[\text{Cu}(\text{L})_2(\text{P}_2\text{Mo}_5\text{O}_{23})] \cdot 4\text{H}_2\text{O}/\text{Fe}_3\text{O}_4$  nanocomposites using organic dyes such as methylene blue, gentian violet, safranin T, fuchsin basic, methyl orange and Sudan red (III) as probe molecules. Fig. 8 show that  $[\text{Cu}(\text{L})_2(\text{H}_2\text{O})]\text{H}_2[\text{Cu}(\text{L})_2(\text{P}_2\text{Mo}_5\text{O}_{23})] \cdot 4\text{H}_2\text{O}/\text{Fe}_3\text{O}_4$  nanocomposites were able to adsorb the methylene blue, gentian violet, safranin T and fuchsin basic efficiently in the dark. The intensity of UV-visible absorption peak of each dyes decreased with the increase of time due to the existence of  $[\text{Cu}(\text{L})_2(\text{H}_2\text{O})]\text{H}_2[\text{Cu}(\text{L})_2(\text{P}_2\text{Mo}_5\text{O}_{23})] \cdot 4\text{H}_2\text{O}/\text{Fe}_3\text{O}_4$  nanocomposites, and the adsorption efficiency

of methylene blue, gentian violet, safranin T and fuchsin basic were 79%, 91%, 64% and 83% in 12 min, 45 min, 60 min and 120 min, respectively. In addition, the peak patterns of each dyes are slightly similar and the peak positions are the same except gentian violet which may be due to itself of gentian violet. Fig. 9 show that  $[\text{Cu}(\text{L})_2(\text{H}_2\text{O})]\text{H}_2[\text{Cu}(\text{L})_2(\text{P}_2\text{Mo}_5\text{O}_{23})] \cdot 4\text{H}_2\text{O}/\text{Fe}_3\text{O}_4$  nanocomposites were not able to adsorb the methyl orange, Sudan red (III) efficiently in the dark. The intensity of UV-visible absorption peak of methyl orange and Sudan red (III) both are almost constant. The reason of the same adsorbent with different effects on removal of dyes is related to the structure of the dye molecules and the structure of the  $[\text{Cu}(\text{L})_2(\text{H}_2\text{O})]\text{H}_2[\text{Cu}(\text{L})_2(\text{P}_2\text{Mo}_5\text{O}_{23})] \cdot 4\text{H}_2\text{O}/\text{Fe}_3\text{O}_4$  nanocomposites.

POMs, as an outstanding family of metal-oxide clusters with controllable shape and size, highly electronegative, and oxo-enriched surfaces, are expected to exhibit good adsorption towards cationic dyes.<sup>44</sup> Firstly, POMs are a kind of hydrophilic metal-oxo cluster compounds. The hydrophilic/hydrophobic property of the framework is modulated by encapsulating the POM molecules, which allows the ingress and egress of the dye molecules. Secondly, POMs with a large number of negative charges encapsulated in the neutral framework may have a stronger force with the positive charges of dyes. The approving

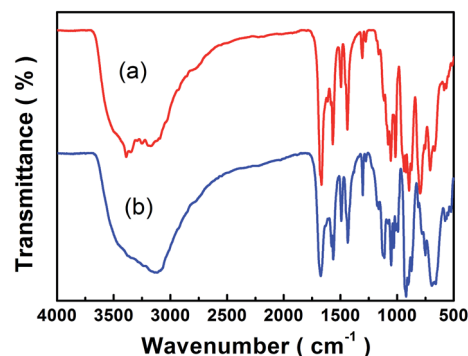


Fig. 10 FTIR spectra as-synthesized (a) and after adsorption and desorption tests (b) of the  $[\text{Cu}(\text{L})_2(\text{H}_2\text{O})]\text{H}_2[\text{Cu}(\text{L})_2(\text{P}_2\text{Mo}_5\text{O}_{23})] \cdot 4\text{H}_2\text{O}/\text{Fe}_3\text{O}_4$  nanocomposites.

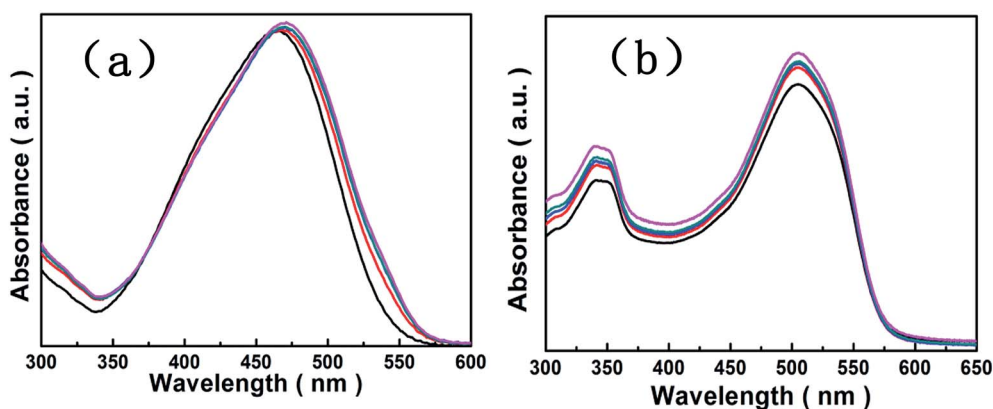


Fig. 9 Adsorption spectra of the methyl orange solution (a) and the Sudan red (III) solution (b) under the dark in presence of the  $[\text{Cu}(\text{L})_2(\text{H}_2\text{O})]\text{H}_2[\text{Cu}(\text{L})_2(\text{P}_2\text{Mo}_5\text{O}_{23})] \cdot 4\text{H}_2\text{O}/\text{Fe}_3\text{O}_4$  nanocomposites.





Fig. 11 The photographs of three adsorption and desorption cycles, the first cycle: Ad-1<sup>st</sup> and De-1<sup>st</sup>, the second cycle: Ad-2<sup>nd</sup> and De-2<sup>nd</sup>, the third cycle: Ad-3<sup>rd</sup> and De-3<sup>rd</sup>.

result is that  $[\text{Cu}(\text{L})_2(\text{H}_2\text{O})]\text{H}_2[\text{Cu}(\text{L})_2(\text{P}_2\text{Mo}_5\text{O}_{23})] \cdot 4\text{H}_2\text{O}/\text{Fe}_3\text{O}_4$  nanocomposites exhibit rapid adsorption efficiency and high uptake capacity towards methylene blue, gentian violet, safranine T and fuchsin basic than methyl orange, Sudan red (III), which is in accord with literature.<sup>45</sup> The magnetic  $[\text{Cu}(\text{L})_2(\text{H}_2\text{O})]\text{H}_2[\text{Cu}(\text{L})_2(\text{P}_2\text{Mo}_5\text{O}_{23})] \cdot 4\text{H}_2\text{O}/\text{Fe}_3\text{O}_4$  nanocomposites combining  $[\text{Cu}(\text{L})_2(\text{H}_2\text{O})]\text{H}_2[\text{Cu}(\text{L})_2(\text{P}_2\text{Mo}_5\text{O}_{23})] \cdot 4\text{H}_2\text{O}$  and  $\text{Fe}_3\text{O}_4$  nanoparticles could be collected in adsorption process preferably.

### 3.9 Stability and reusability behaviours

The stability and reusability of the nanocomposites are another important standard for practical application. It can be seen from the process of magnetic aggregation and dispersion that the  $[\text{Cu}(\text{L})_2(\text{H}_2\text{O})]\text{H}_2[\text{Cu}(\text{L})_2(\text{P}_2\text{Mo}_5\text{O}_{23})] \cdot 4\text{H}_2\text{O}/\text{Fe}_3\text{O}_4$  are not the mixture of  $[\text{Cu}(\text{L})_2(\text{H}_2\text{O})]\text{H}_2[\text{Cu}(\text{L})_2(\text{P}_2\text{Mo}_5\text{O}_{23})] \cdot 4\text{H}_2\text{O}$  and  $\text{Fe}_3\text{O}_4$  nanoparticles but a new nanocomposite, although it is still a challenge to identify the interaction between POM species and magnetic particles. The in-depth study is on the way. As shown in Fig. 10, the IR patterns of the adsorbents regenerated from adsorption and desorption experiments match well with the as-synthesized product, indicating that the structure of the nanocomposites remain intact, which confirms their good stability and recyclability. The properties are significant in improving the use of material without loss of their structure and reducing the adsorption cost. In a word, the nanocomposites are of great significance for the practical use of the absorbents and exhibit good reproducibility.

After adsorption experiments, the adsorbed fuchsin basic can be removed by a solvent DMF. In Fig. 11, it shows that the photographs of three adsorption and desorption cycles. When a solution of DMF was added, digital images show that fuchsin basic molecules in the nanocomposites can be rapidly released. Then, the regenerated  $[\text{Cu}(\text{L})_2(\text{H}_2\text{O})]\text{H}_2[\text{Cu}(\text{L})_2(\text{P}_2\text{Mo}_5\text{O}_{23})] \cdot 4\text{H}_2\text{O}/\text{Fe}_3\text{O}_4$  nanocomposites were added to the initial fuchsin basic solution (20 mL of  $15 \text{ mg L}^{-1}$ ), the adsorbents are still capable of removing fuchsin basic up to 91%, 93% and 90% over one cycles, two cycle, three cycle, respectively, as shown in Fig. 12. This means that the dye release is also an ion-exchange process, which also further demonstrate that ionic interaction between dyes and anionic framework is main determinant for selective adsorption and separation of dyes.<sup>46</sup>

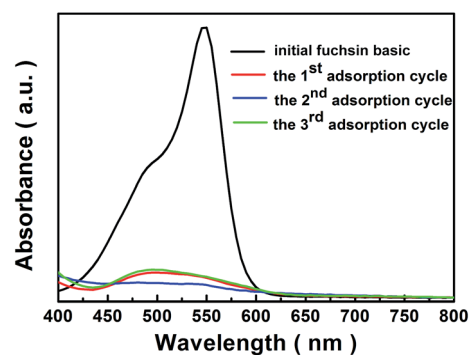


Fig. 12 The UV-vis spectra of initial fuchsin basic, the 1<sup>st</sup> adsorption cycle, the 2<sup>nd</sup> adsorption cycle and the 3<sup>rd</sup> adsorption cycle.

The new  $[\text{Cu}(\text{L})_2(\text{H}_2\text{O})]\text{H}_2[\text{Cu}(\text{L})_2(\text{P}_2\text{Mo}_5\text{O}_{23})] \cdot 4\text{H}_2\text{O}/\text{Fe}_3\text{O}_4$  nanocomposites have been successfully synthesized, and were adopted as adsorbents for the removal of dyes in aqueous solution. Interestingly, they not only exhibit rapid adsorption rate and high uptake capacity towards fuchsin basic, but also realize the recycling performance. This work opens up a useful, economical adsorption and desorption, which can improve the recycling of raw material in wastewater.

## 4 Conclusions

In summary, we have successfully synthesized the nanocomposites of  $[\text{Cu}(\text{L})_2(\text{H}_2\text{O})]\text{H}_2[\text{Cu}(\text{L})_2(\text{P}_2\text{Mo}_5\text{O}_{23})] \cdot 4\text{H}_2\text{O}/\text{Fe}_3\text{O}_4$  that combining  $[\text{Cu}(\text{L})_2(\text{H}_2\text{O})]\text{H}_2[\text{Cu}(\text{L})_2(\text{P}_2\text{Mo}_5\text{O}_{23})] \cdot 4\text{H}_2\text{O}$  and  $\text{Fe}_3\text{O}_4$  nanoparticles. The morphology and structural analyses reveal the narrow particle size distribution with an average diameter  $\sim 19.43 \text{ nm}$  and high crystallinity of the nanocomposite. The FTIR and XRD assessments confirm  $[\text{Cu}(\text{L})_2(\text{H}_2\text{O})]\text{H}_2[\text{Cu}(\text{L})_2(\text{P}_2\text{Mo}_5\text{O}_{23})] \cdot 4\text{H}_2\text{O}$  and  $\text{Fe}_3\text{O}_4$  nanoparticles are existed in  $[\text{Cu}(\text{L})_2(\text{H}_2\text{O})]\text{H}_2[\text{Cu}(\text{L})_2(\text{P}_2\text{Mo}_5\text{O}_{23})] \cdot 4\text{H}_2\text{O}/\text{Fe}_3\text{O}_4$  nanocomposites. The UV-vis measurement shows the well-defined optical absorption with the nanocomposites dispersed in  $\text{H}_2\text{O}$ . The magnetic characterization shows that  $[\text{Cu}(\text{L})_2(\text{H}_2\text{O})]\text{H}_2[\text{Cu}(\text{L})_2(\text{P}_2\text{Mo}_5\text{O}_{23})] \cdot 4\text{H}_2\text{O}/\text{Fe}_3\text{O}_4$  nanocomposites have superparamagnetic behavior. The dispersion-collection processes in  $\text{H}_2\text{O}$  of the  $[\text{Cu}(\text{L})_2(\text{H}_2\text{O})]\text{H}_2[\text{Cu}(\text{L})_2(\text{P}_2\text{Mo}_5\text{O}_{23})] \cdot 4\text{H}_2\text{O}/\text{Fe}_3\text{O}_4$  nanocomposites were





demonstrated for application readiness.  $[\text{Cu}(\text{L})_2(\text{H}_2\text{O})]\text{H}_2\text{O}$ – $[\text{Cu}(\text{L})_2(\text{P}_2\text{Mo}_5\text{O}_{23})]\cdot 4\text{H}_2\text{O}/\text{Fe}_3\text{O}_4$  nanocomposites have selective adsorption behavior for organic dyes. Meanwhile, the stable and reusable  $[\text{Cu}(\text{L})_2(\text{H}_2\text{O})]\text{H}_2\text{O}$ – $[\text{Cu}(\text{L})_2(\text{P}_2\text{Mo}_5\text{O}_{23})]\cdot 4\text{H}_2\text{O}/\text{Fe}_3\text{O}_4$  nanocomposites were found to be a good adsorbent and could be employed as an effective adsorbent applicable in adsorption field.

## Acknowledgements

This work was supported in part by the National Natural Science Foundation of China (no. 5117206 and 21671055) and the Key Scientific Research Projects of Henan Province Colleges and Universities, Foundation of Education Department of Henan Province, China (no. 16A150002).

## References

- 1 Z. Ma, Q. Liu, Z. M. Cui, S. W. Bian and W. G. Song, *J. Phys. Chem. C*, 2008, **112**, 8875–8880.
- 2 M. Huang, L. Bi, Y. Shen, B. Liu and S. Dong, *J. Phys. Chem. B*, 2004, **108**, 9780–9786.
- 3 Z. Sun, L. Xu, W. Guo, B. Xu, S. Liu and F. Li, *J. Phys. Chem. C*, 2010, **114**(11), 5211–5216.
- 4 C. Li, K. P. O'Halloran, H. Ma and S. Shi, *J. Phys. Chem. B*, 2009, **113**, 8043–8048.
- 5 J. Kim, L. Lee, B. K. Niece, J. X. Wang and A. A. Gewirth, *J. Phys. Chem. B*, 2004, **108**, 7927–7933.
- 6 D. An, A. Ye, W. Deng, Q. Zhang and Y. Wang, *Chem.–Eur. J.*, 2012, **18**, 2938–2947.
- 7 S. Li, X. Yu, G. Zhang, Y. Ma, J. Yao and P. de Oliveira, *Carbon*, 2011, **49**, 1906–1911.
- 8 A. Troupis, A. Hiskia and E. Papaconstantinou, *Angew. Chem., Int. Ed.*, 2002, **41**(11), 1911–1914.
- 9 E. Tebandeke, C. Coman, K. Guillois, G. Canning, E. Ataman, J. Knudsen, L. R. Wallenberg, H. Ssekaalo, J. Schnadt and O. F. Wendt, *Green Chem.*, 2014, **16**, 1586–1593.
- 10 A. Babakhanian, S. Kaki, M. Ahmadi, H. Ehzari and A. Pashabadi, *Biosens. Bioelectron.*, 2014, **60**, 185–190.
- 11 H. K. Daima, P. R. Selvakannan, R. Shukla, S. K. Bhargava and V. Bansal, *PLoS One*, 2013, **8**, e79676.
- 12 W. Zheng, L. Yang, Y. Liu, X. Qin, Y. Zhou, Y. Zhou and J. Liu, *Sci. Technol. Adv. Mater.*, 2014, **15**, 035010.
- 13 Y. Kikukawa, Y. Kuroda, K. Yamaguchi and N. Mizuno, *Angew. Chem.*, 2012, **124**, 2484–2487.
- 14 U. Kortz, A. Müller, J. van Slageren, J. Schnack, N. S. Dalal and M. Dressel, *Coord. Chem. Rev.*, 2009, **253**, 2315–2327.
- 15 H. N. Miras, J. Yan, D. L. Long and L. Cronin, *Chem. Soc. Rev.*, 2012, **41**, 7403–7430.
- 16 K. M. Seemann, M. Luysberg, Z. Révay, P. Kudejova, B. Sanz, N. Cassinelli, A. Loidl, K. Llicic, G. Multhoff and T. E. Schmid, *J. Controlled Release*, 2015, **197**, 131–137.
- 17 Z. You, Y. Chen, T. Liu, Z. Yang, F. Xie and Y. Sun, *Inorg. Chim. Acta*, 2014, **421**, 160–168.
- 18 S. Saif, A. Tahir and Y. Chen, *Nanomaterials*, 2016, **6**, 209.
- 19 H. L. Liu, J. H. Wu, J. H. Min and Y. K. Kim, *J. Alloys Compd.*, 2012, **537**, 60–64.
- 20 H. L. Liu, J. H. Wu, J. H. Min, X. Y. Zhang and Y. K. Kim, *Mater. Res. Bull.*, 2013, **48**, 551–558.
- 21 H. L. Liu, P. Hou, W. X. Zhang and J. H. Wu, *Colloids Surf.*, 2010, **356**(1), 21–27.
- 22 H. L. Liu, S. P. Ko, J. H. Wu, M. H. Jung, J. H. Min, J. H. Lee, B. H. An and Y. K. Kim, *J. Magn. Magn. Mater.*, 2007, **310**(2), e815–e817.
- 23 S. Lin, Z. Song, G. Che, A. Ren, P. Li, C. Liu and J. Zhang, *Microporous Mesoporous Mater.*, 2014, **193**, 27–34.
- 24 A. Dandia, V. Parewa, A. K. Jain and K. S. Rathore, *Green Chem.*, 2011, **13**, 2135.
- 25 B. Adhikari, G. Palui and A. Banerjee, *Soft Matter*, 2009, **5**, 3452–3460.
- 26 J. Thomas and A. Ramanan, *Inorg. Chim. Acta*, 2011, **372**, 243–249.
- 27 M. Đaković, Z. Popović, G. Giester and M. Rajić-Linarić, *Polyhedron*, 2008, **27**, 210–222.
- 28 H. Paşaoğlu, S. Güven, Z. Heren and O. Büyükgüngör, *J. Mol. Struct.*, 2006, **794**, 270–276.
- 29 G. M. Sheldrick, *Acta Crystallogr., Sect. A: Found. Crystallogr.*, 2008, **64**(1), 112–122.
- 30 J. X. Meng, Y. Lu, Y. G. Li, H. Fu and E. B. Wang, *CrystEngComm*, 2011, **13**, 2479–2486.
- 31 H. J. Jin, B. B. Zhou, Y. Yu, Z. F. Zhao and Z. H. Su, *CrystEngComm*, 2011, **13**, 585–590.
- 32 R. Yuvakkumar and S. I. Hong, *Adv. Mater. Res.*, 2014, **1051**, 39–42.
- 33 Y. P. Yew, K. Shameli, M. Miyake, N. Kuwano, N. B. B. A. Khairudin, S. E. B. Mohamad and K. X. Lee, *Nanoscale Res. Lett.*, 2016, **11**(1), 1–7.
- 34 S. H. Ahmadi, P. Davar and A. Manbohi, *Iran. J. Chem. Chem. Eng.*, 2016, **35**, 63–73.
- 35 Z. L. Li, Y. Wang, L. C. Zhang, J. P. Wang, W. S. You and Z. M. Zhu, *Dalton Trans.*, 2014, **43**, 5840–5846.
- 36 B. D'Cruz, J. Samuel and L. George, *Thermochim. Acta*, 2014, **596**, 29–36.
- 37 L. H. Wei, Z. L. Wang, J. W. Zhao and J. P. Wang, *Chin. J. Struct. Chem.*, 2010, **29**, 784–788.
- 38 G. Zhang, B. Keita, A. Dolbecq, P. Mialane, F. Sécheresse, F. Miserque and L. Nadjo, *Chem. Mater.*, 2007, **19**, 5821–5823.
- 39 A. Neyman, L. Meshi, L. Zeiri and I. A. Weinstock, *J. Am. Chem. Soc.*, 2008, **130**, 16480–16481.
- 40 H. L. Liu, J. H. Wu, J. H. Min, P. Hou, A. Y. Song and Y. K. Kim, *Nanotechnology*, 2010, **22**, 055701.
- 41 S. Thakur, S. Pandey and O. A. Arotiba, *Carbohydr. Polym.*, 2016, **153**, 34–46.
- 42 K. A. G. Gusmão, L. V. A. Gurgel, T. M. S. Melo and L. F. Gil, *J. Environ. Manage.*, 2013, **118**, 135–143.
- 43 X. Xu, B. Bai, H. Wang and Y. Suo, *J. Phys. Chem. Solids*, 2015, **87**, 23–31.
- 44 A. X. Yan, S. Yao, Y. G. Li, Z. M. Zhang, Y. Lu, W. L. Chen and E. B. Wang, *Chem.–Eur. J.*, 2014, **20**, 6927–6933.
- 45 F. Y. Yi, W. Zhu, S. Dang, J. P. Li, D. Wu, Y. H. Li and Z. M. Sun, *Chem. Commun.*, 2015, **51**, 3336–3339.
- 46 J. S. Qin, S. R. Zhang, D. Y. Du, P. Shen, S. J. Bao, Y. Q. Lan and Z. M. Su, *Chem.–Eur. J.*, 2014, **20**, 5625–5630.

